

# A Modularization Method for Battery Equalizers Using Multiwinding Transformers

Yunlong Shang<sup>1</sup>, Student Member, IEEE, Bing Xia, Student Member, IEEE, Chenghui Zhang<sup>2</sup>, Member, IEEE, Naxin Cui, Member, IEEE, Jufeng Yang, Student Member, IEEE, and Chris Mi<sup>3</sup>, Fellow, IEEE

**Abstract**—This paper proposes a modularized global architecture using multi-winding transformers for battery cell balancing. The global balancing for a series-connected battery string is achieved based on forward conversion in each battery module and based on flyback conversion among modules. The demagnetization of the multiwinding transformers is also simultaneously achieved by the flyback conversion among modules without the need of additional demagnetizing circuits. Moreover, all MOSFET switches are driven by two complementary pulse width modulation signals without the requirement of cell voltage sensors, and energy can be automatically and simultaneously delivered from any high voltage cells to any low voltage cells. Compared with existing equalizers requiring additional balancing circuits for battery modules, the proposed modularized equalizer shares one circuit for the balancing among cells and modules. The balancing performance of the proposed equalizer is perfectly verified through experimental results, and the maximum balancing efficiency is up to 91.3%. In summary, the proposed modularized equalizer has the advantages of easier modularization, simpler control, higher efficiency, smaller size, and lower cost, ensuring the battery system higher reliability and easier implementation.

**Index Terms**—Electric vehicles (EVs), forward conversion, flyback conversion, lithium-ion batteries, multi-winding transformers, modularized equalizers.

Manuscript received October 1, 2016; revised March 12, 2017; accepted April 23, 2017. Date of publication May 9, 2017; date of current version October 13, 2017. This work was supported in part by the Major Scientific Instrument Development Program of the National Natural Science Foundation of China under Grant 61527809, in part by the Key Project of National Natural Science Foundation of China under Grant 61633015, in part by the Key Research and Development Program of Shandong Province under Grant 2016ZDJS03A02, in part by the Nanjing Golden Dragon Bus Co., Ltd., in part by the US Department of Energy under the Graduate Automotive Technology Education Center program, and in part by the China Scholarship Council. The review of this paper was coordinated by A. Chatterjee. (Corresponding author: Chunting Chris Mi.)

Y. Shang is with the School of Control Science and Engineering, Shandong University, Jinan 250061, China, and also with the Department of Electrical and Computer Engineering, San Diego State University, San Diego, CA 92182 USA (e-mail: shangyunlong@mail.sdu.edu.cn).

B. Xia is with the Department of Electrical and Computer Engineering, San Diego State University, San Diego, CA 92182 USA, and also with the Department of Electrical and Computer Engineering, University of California San Diego, CA 92093 USA (e-mail: bixia@eng.ucsd.edu).

C. Zhang and N. Cui are with the School of Control Science and Engineering, Shandong University, Jinan 250061, China (e-mail: zchui@sdu.edu.cn; cuiinx@sdu.edu.cn).

J. Yang is with the Department of Electrical Engineering, Nanjing University of Aeronautics and Astronautics, Nanjing 211106, China, and also with the Department of Electrical and Computer Engineering, San Diego State University, San Diego, CA 92182 USA (e-mail: nuaayjf@163.com).

C. Mi is with the Department of Electrical and Computer Engineering, San Diego State University, San Diego, CA 92182 USA (e-mail: mi@ieee.org).

Color versions of one or more of the figures in this paper are available online at <http://ieeexplore.ieee.org>.

Digital Object Identifier 10.1109/TVT.2017.2702065

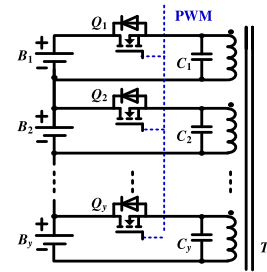


Fig. 1. The battery balancing circuit using a single multi-winding transformer based on forward conversion [28].

## I. INTRODUCTION

LITHIUM-ION battery has the advantages of low self-discharge rate, high energy density, long lifetime, high cell voltage, and no memory effect, and is currently deemed to be one of the most widespread rechargeable batteries [1]–[2]. It has been widely used in many fields, such as electric vehicles (EVs) [3]–[4]. However, the inconsistency caused by manufacturing and environment leads to the unfavorable tolerances of the capacities and internal resistances of battery cells [5]–[6]. Generally, hundreds or even thousands of battery cells are connected in series and parallel to construct a battery pack in order to meet the voltage and capacity requirements of loads. However, the inconsistency of battery cells will cause the cell voltage imbalance as the repetitive charging and discharging for the battery pack. In fact, charging or discharging the cells outside of their allowable voltage range would result in battery failure, even explosion or fire, while bounding charging and discharging when any cell in the battery pack reaches its maximum or minimum voltage cannot make full use of the energy of the battery string [6]. Therefore, battery equalizers are required in order to compensate these imbalances and fully use the energy of the battery string.

There have been numerous developments in battery equalizers during the last few years, such as shunt resistor [7], switched capacitors [8]–[13], zero-current switching (ZCS) switched capacitors [14]–[18], buck-boost converters [19]–[21], flyback converters [22]–[25], forward converters [26]–[28], and forward-flyback converters [29]–[31]. Among these topologies, transformer-based solutions [22]–[31] have the advantages of high efficiency, simple control, and easy isolation. For example, Li *et al.* [28] proposes a battery equalizer using multi-winding transformers based on forward conversion. As shown in Fig. 1,

one MOSFET switch, one winding of a multi-winding transformer, and one capacitor are needed for each cell. The biggest advantage of this topology is that energy can be directly transferred from any higher-voltage cells to any lower-voltage cells by driving the MOSFETs using one PWM signal. However, the multi-winding transformer has the problems of mismatching, bulk size, and high complexity implementation, which is difficult to be applied to a long battery string with hundreds of cells connected in series. Moreover, the mismatched multi windings will lead to a natural imbalance among cell voltages. Fortunately, these problems can be overcome by the modularization [32]–[33], for which a long battery string is divided into  $x$  modules with  $y$  cells in each module. Fig. 2(a) shows the module-based architecture for battery equalizers, where an intra-module and inter-module equalizers are employed to achieve the global equalization. However, this solution needs additional stage circuits to balance among modules, resulting in bulky size, high cost, energy loss, and high voltage stress on MOSFETs. In order to remove the inter-module circuits, a parallel architecture is proposed, as shown in Fig. 2(b), which utilizes the magnetizing energy of the transformers to transfer energy among modules. However, a dedicated demagnetizing circuit (including a winding and a diode, as shown by the green lines) is still mandatory for each module, resulting in the low efficiency, bulk size, mismatching, complex design, and difficult implementation.

To solve these problems, a modularized automatic equalizer (MAE) using multi-winding transformers is proposed in this paper. The battery string is divided into  $x$  battery modules with  $y$  cells in each module. One symmetrical multi-winding transformer is set for each battery module, and all the secondary windings of the transformers are connected in parallel. Nevertheless, the secondary windings of the odd modules have the opposite polarities compared with those of the even modules. Because of these configurations, the global equalization is achieved based on forward conversion in each battery module and flyback conversion among the modules. Moreover, the demagnetization for the transformers is also achieved by the flyback conversion among the modules without the need of additional demagnetizing circuits. By controlling the MOSFETs using two complementary PWM signals, the proposed MAE can transfer automatically and simultaneously energy from any higher voltage cells to any lower voltage cells without the need of cell voltage sensors. This system has the advantages of smaller size, lower cost, lower voltage stress, and easier modularization compared with existing methods, which makes the proposed MAE be a feasible solution for EVs.

## II. THE PROPOSED MODULARIZED EQUALIZER

In this paper, a modularized global architecture for battery equalization is presented, which is a modularization method of the work in [28]. The global equalization is achieved based on forward and flyback conversion without the needs of inter-module equalizers, demagnetizing circuits, and cell voltage detectors.

### A. Configuration of the Proposed MAE

Fig. 3 shows the schematic diagram of the proposed MAE applied to a long battery string, which is divided into  $x$  modules with  $y$  cells in each module. The proposed MAE consists of two parts: the primary sides and the secondary sides. Each primary winding of a multi-winding transformer connects a MOSFET and a battery cell. The primary windings of each multi-winding transformer have the same polarities, which are implemented by the conventional forward converters. The main function of this stage is to balance the cell voltages in each battery module based on forward conversion. The secondary sides of all the transformers are connected in parallel, and they have the same polarities for the odd/even transformers, which are also implemented by the conventional forward converters. Nevertheless, the secondary sides of the odd transformers have the opposite polarities compared with the even ones, which are implemented by the conventional flyback converters. This complementary configuration achieves the global equalization for the battery string, and obtains the demagnetization for all the transformers based on flyback conversion.

The unique characteristics of the proposed MAE are as follows:

- 1) Only one MOSFET switch and one primary winding are needed for each cell, thereby leading to smaller size and lower cost compared with existing equalizers.
- 2) Demagnetizing circuits are not necessary because the magnetizing energy can be automatically reset through the complementary structures of the secondary sides of the transformers.
- 3) By controlling the MOSFET switches using two PWM signals with complementary states, automatic any-cells-to-any-cells balancing is achieved without the requirement of cell voltage sensors.
- 4) The balancing operation in each module is based on forward conversion, while the balancing operation among the modules is based on flyback conversion, by which the global equalization for the battery string is achieved without the need of inter-module equalizers.
- 5) Due to the effective demagnetization for the transformers, a low voltage stress on the power devices are achieved, thereby ensuring a high reliability of the equalization circuit.

### B. Operation Principles

By driving the MOSFETs using two complementary PWM signals for the odd and even modules, the proposed equalizer can achieve the global automatic balancing among cells without the requirement of cell monitoring circuits. The proposed equalizer works on the forward and flyback operations. The forward operation is employed to achieve the voltage equalization in each battery module. The flyback operation is employed to achieve the voltage equalization among the modules, and reset the magnetic energy stored in the transformers. In order to simplify the analysis for the operation modes, the following assumptions are made:

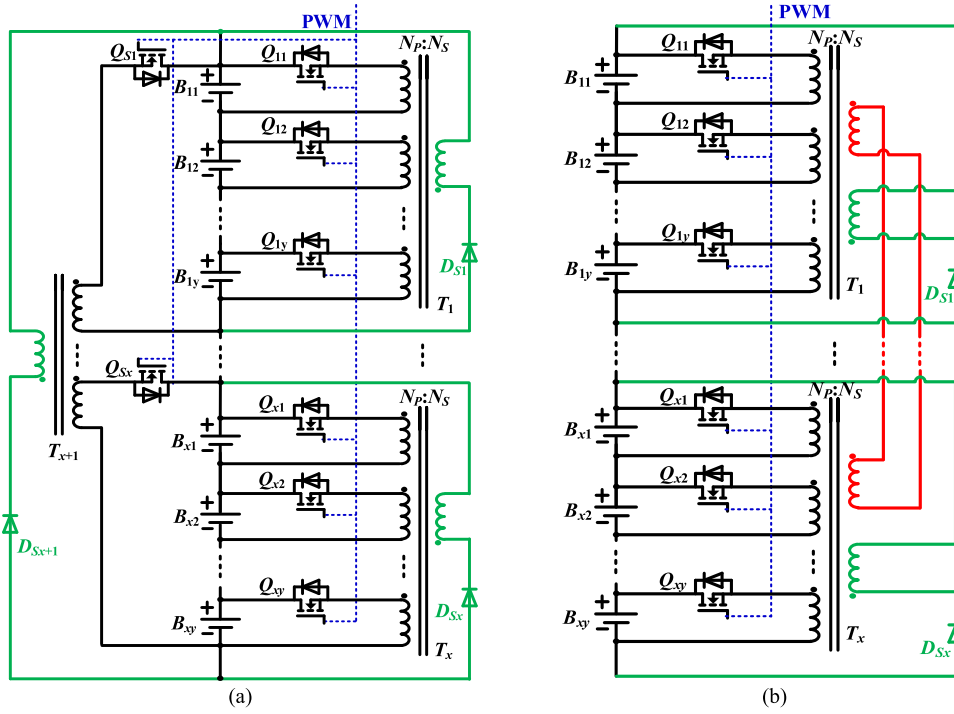


Fig. 2. Architectures of the modularized equalizers for a long battery string [32]. (a) The module-based architecture. (b) The parallel architecture.

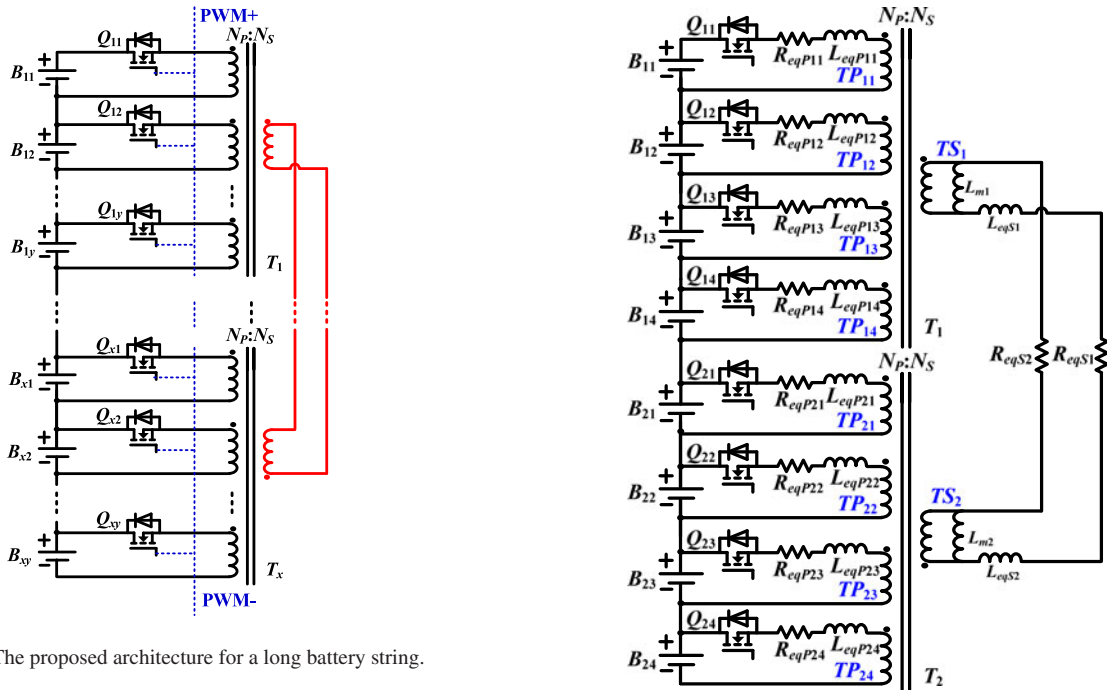


Fig. 3. The proposed architecture for a long battery string.

Fig. 4. The equivalent circuit of the proposed two-module equalizer.

- 1) The modularization concept is applied to a battery string of eight cells, which is modularized into two separate modules,  $M_1$  and  $M_2$ , including four cells in each module. Fig. 4 shows the equivalent circuit of the proposed two-module equalizer.
- 2) The transformers have the same parameters, e.g., the same turn number, magnetizing inductance, leakage inductance, and equivalent resistance of each winding.
- 3) A PWM signal  $PWM+$  is applied to all switches in Module I, and the complementary PWM signal  $PWM-$  is applied to all switches in Module II.
- 4) The initial cell voltages meet  $V_{B24} > V_{B23} > V_{B22} > V_{B21} > V_{B14} > V_{B13} > V_{B12} > V_{B11}$ . Therefore, the voltage of Module II ( $V_{M2} = V_{B24} + V_{B23} + V_{B22} + V_{B21}$ ) is higher than the voltage of Module I ( $V_{M1} = V_{B14} + V_{B13} + V_{B12} + V_{B11}$ ).

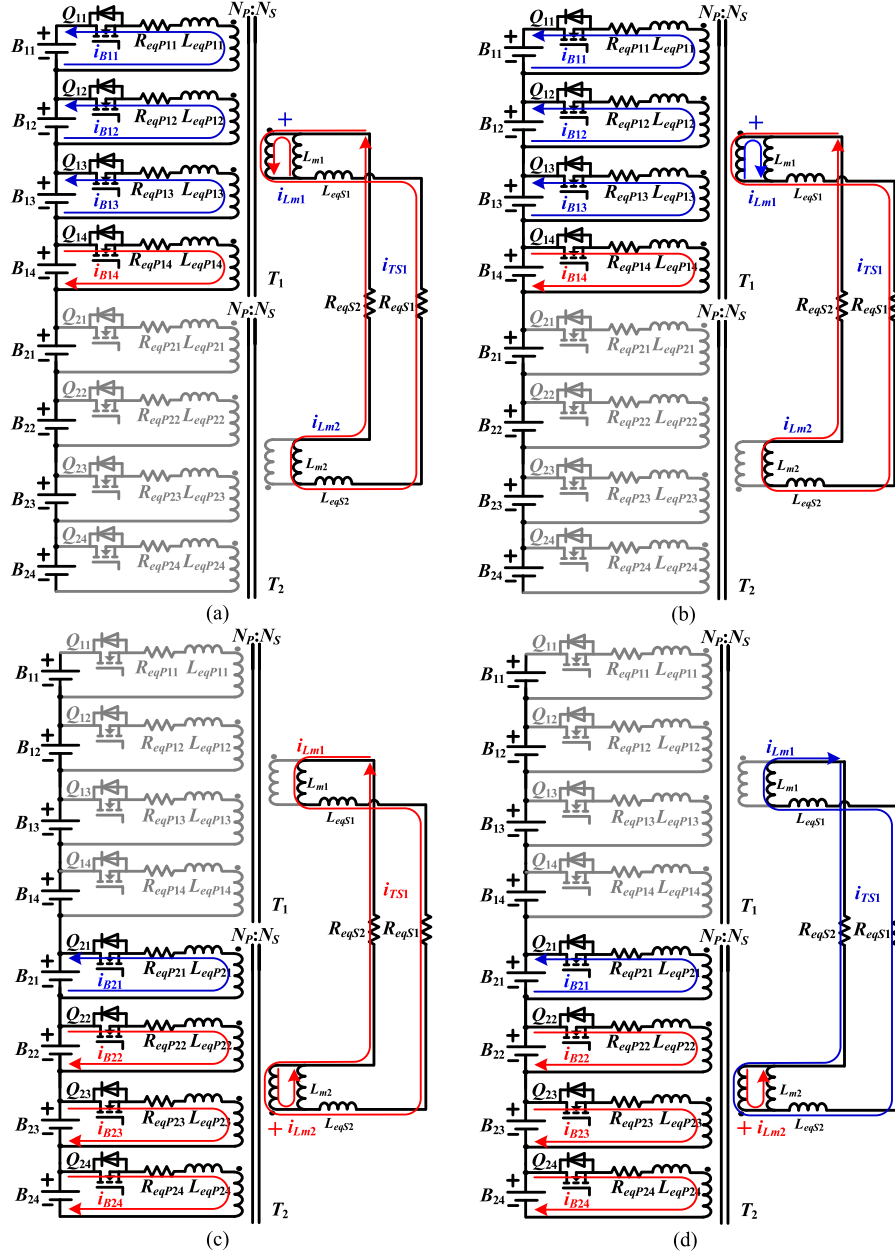


Fig. 5. Operating modes of the proposed equalizer. (a) Mode I. (b) Mode II. (c) Mode III. (d) Mode IV.

- 5) It is specified that the current flowing into a battery cell is positive, otherwise is negative. The secondary balancing current flowing into the dotted terminal of Transformer I is positive, otherwise is negative.

In the steady state, there are four operating modes during one switching period. Figs. 5 and 6 present the operating modes and the theoretical waveforms, respectively.

**Mode I** ( $t_0 - t_1$ ): At  $t_0$ , all switches  $Q_{21} - Q_{24}$  in Module II are turned off, and all switches  $Q_{11} - Q_{14}$  in Module I are turned on.

The balancing currents in the primary sides of Module II drop instantaneously to zero at  $t_0$ , and the reset current is built up in the secondary sides of the transformers. The balancing currents among cells in the primary sides of Module I flow automatically through switches  $Q_{11} - Q_{14}$  based on forward conversion, as

shown in Fig. 5(a). Due to  $V_{B14} > V_{B13} > V_{B12} > V_{B11}$ , it can be reasonably assumed that  $i_{B14}$  flows from the cells to the transformer, and  $i_{B11}, i_{B12}, i_{B13}$  flow from the transformer to the cells. A larger current flows into the lower voltage cells, and a smaller current flows into the higher voltage cells, by which the any-cells-to-any-cells equalization for Module I is automatically achieved based on forward conversion.

During this mode, the primary voltages of Transformer I  $V_{TP1j}$  can be expressed as

$$V_{TP1j} = V_{B1j} + L_{eqP1j} \cdot \frac{di_{B1j}}{dt} + R_{eqP1j} \cdot i_{B1j}, \quad (1)$$

where  $j = 1, 2, \dots, 4$ .  $V_{B1j}$  is the cell voltage of  $B_{1j}$  in Module I.  $i_{B1j}$  is the balancing current of  $B_{1j}$ .  $L_{eqP1j}$  represents the leakage inductance on a primary winding of Transformer I.

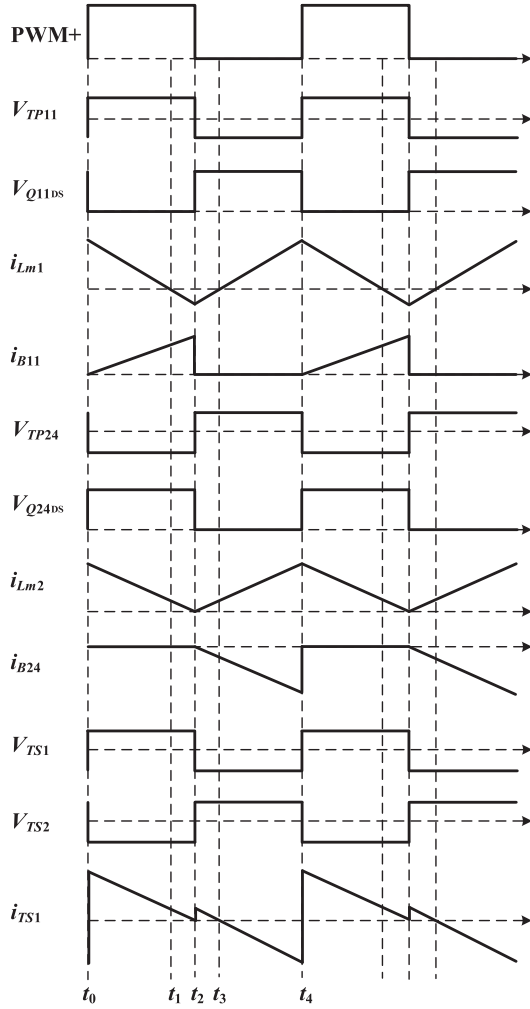


Fig. 6. Key waveforms of the proposed modularized equalizer.

$R_{eqP1j}$  represents the equivalent resistance on a primary winding of Transformer I. According to Faraday's law, the primary windings of the transformers should have the same turn number to achieve the equalization among cells in a battery module. Thus, the primary voltages of Transformer I satisfy

$$V_{TP1} = V_{TP11} = V_{TP12} = V_{TP13} = V_{TP14} = \frac{V_{M1}}{4}, \quad (2)$$

where  $V_{TP1}$  represents the uniform primary voltage of Transformer I.

By solving (1), the primary balancing current  $i_{B1j}(t)$  is derived as

$$i_{B1j}(t) \approx \frac{V_{M1} - 4V_{B1j}}{4L_{eqP1j}} \cdot (t - t_0). \quad (3)$$

Since the voltage difference between  $V_{TP1j}$  and  $V_{B1j}$  is applied to leakage inductance  $L_{eqP1j}$ , balancing current  $i_{B1j}$  rises linearly from zero, as shown in Fig. 6.

The loop equation in the secondary sides of the transformers can be represented by

$$V_{TS1} + V_{TS2} + (L_{eqS1} + L_{eqS2}) \cdot \frac{di_{TS1}}{dt} + (R_{eqS1} + R_{eqS2}) \cdot i_{TS1} = 0, \quad (4)$$

where  $i_{TS1}$  is the secondary balancing current.  $L_{eqS1}$  and  $L_{eqS2}$  represent the leakage inductances on the secondary windings of Transformer I and Transformer II, respectively.  $R_{eqS1}$  and  $R_{eqS2}$  represent the equivalent resistances on the secondary windings of Transformer I and Transformer II, respectively.  $V_{TS1}$  and  $V_{TS2}$  represent the secondary voltages of Transformer I and Transformer II, respectively, which are determined by

$$V_{TS1} = \frac{N_S}{N_P} \cdot V_{TP1} = \frac{n}{4} \cdot V_{M1}, \quad (5)$$

$$V_{TS2} = \frac{N_S}{N_P} \cdot V_{TP2} = -\frac{n}{4} \cdot V_{M2}, \quad (6)$$

where  $N_P$  is the turn number of the primary windings of the transformers.  $N_S$  is the turn number of the secondary windings of the transformers.  $V_{TP2}$  represents the uniform primary voltage of Transformer II.  $n$  is the turns ratio of the transformers, which can be expressed as

$$n = \frac{N_S}{N_P}. \quad (7)$$

From (4), (5), and (6), the primary voltages of Transformer II can be calculated as

$$V_{TP2j} = V_{TP2} = -V_{TP1} - \frac{N_P}{N_S} \cdot (L_{eqS1} + L_{eqS2}) \cdot \frac{di_{TS1}}{dt} - \frac{N_P}{N_S} \cdot (R_{eqS1} + R_{eqS1}) \cdot i_{TS1}, \quad (8)$$

where  $j = 1, 2, \dots, 4$ . When the secondary balancing current  $i_{TS1}$  drops to zero, (8) can be simplified as

$$V_{TP2} = -V_{TP1}. \quad (9)$$

This equation shows the equalization between modules can be achieved in theory.

As shown in Fig. 5(a), the secondary balancing current  $i_{TS1}$  changes instantaneously its direction at  $t_0$ , which demagnetizes the second transformer when  $Q_{21} - Q_{24}$  are turned off. The energy stored in the magnetizing inductances of  $L_{m1}$  and  $L_{m2}$  during the last mode is transferred to the cells in Module I based on flyback conversion, which achieves the equalization between the two modules. By solving (4), the secondary balancing current  $i_{TS1}(t)$  can be approximately derived as

$$i_{TS1}(t) \approx i_{TS1}(t_0) - \frac{n}{4} \cdot \frac{V_{M2} - V_{M1}}{L_{eqS1} + L_{eqS2}} \cdot (t - t_0). \quad (10)$$

Since  $V_{M2} - V_{M1} > 0$ ,  $i_{TS1}(t)$  will decrease linearly with a constant slope, as shown in Fig. 6.

During this mode, the magnetizing currents  $i_{L_{m1}}(t)$  and  $i_{L_{m2}}(t)$  in Transformer I and Transformer II can be determined by

$$i_{L_{m1}}(t) = i_{L_{m1}}(t_0) - \frac{n}{4} \cdot \frac{V_{M1}}{L_{m1}} \cdot (t - t_0), \quad (11)$$

$$i_{L_{m2}}(t) = i_{L_{m2}}(t_0) - \frac{n}{4} \cdot \frac{V_{M2}}{L_{m2}} \cdot (t - t_0), \quad (12)$$

Since the secondary voltages are reversely applied to the magnetizing inductances  $L_{m1}$  and  $L_{m2}$ , magnetization currents  $i_{L_{m1}}(t)$  and  $i_{L_{m2}}(t)$  will decrease linearly with a constant slope, as shown in Fig. 6.

As shown in Fig. 5(a), the secondary balancing current  $i_{TS1}$  comes completely from the magnetizing current  $i_{L_{m2}}$  of Transformer II, so we have

$$i_{TS1} = i_{L_{m2}}. \quad (13)$$

The relationship among the magnetizing currents and the balancing currents in Module I can be expressed as

$$\frac{N_S}{N_P} \cdot (i_{L_{m1}} + i_{L_{m2}}) = \sum_{j=1}^4 i_{B1j}. \quad (14)$$

The main function of this mode is to balance the cell voltages of Module I, deliver the energy stored in magnetizing inductances  $L_{m1}$  and  $L_{m2}$  to Module I, and achieve the demagnetization of the second transformer when switches  $Q_{21} - Q_{24}$  are turned off.

**Mode II ( $t_1 - t_2$ ):** At  $t_1$ , magnetization current  $i_{L_{m1}}$  drops to zero, and then increases in reverse direction, which can be expressed as

$$i_{L_{m1}}(t) \approx -\frac{n}{4} \cdot \frac{V_{M1}}{L_{m1}} \cdot (t - t_1). \quad (15)$$

This shows that the energy of Module I is stored in magnetizing inductance  $L_{m1}$ , as shown in Fig. 5(b).

During this mode, the magnetization current  $i_{L_{m2}}$  in Module II continues to decrease linearly, and will drop to zero at  $t_2$ . The cell equalization in the primary sides of Module I still goes on.

This mode is a transition stage that provides pre-conditions for the demagnetization of the first transformer when  $Q_{11} - Q_{14}$  are turned off.

**Mode III ( $t_2 - t_3$ ):** At  $t_2$ , all switches  $Q_{11} - Q_{14}$  in Module I are turned off, and all switches  $Q_{21} - Q_{24}$  in Module II are turned on.

The balancing currents in the primary sides of Module I drop instantaneously to zero at  $t_2$ , and the reset current is built up in the secondary sides of the transformers. The balancing currents in the primary sides of Module II flows automatically through  $Q_{21} - Q_{24}$  based on forward conversion, as shown in Fig. 5(c). Due to  $V_{B24} > V_{B23} > V_{B22} > V_{B21}$ , it is reasonably assumed that  $i_{B21}$  flows from the second transformer to the cell  $B_{21}$ , while  $i_{B22}$ ,  $i_{B23}$ , and  $i_{B24}$  flow from the cells to the transformer. This means that energy in  $B_{22}$ ,  $B_{23}$ , and  $B_{24}$  is simultaneously transferred to  $B_{21}$ . A larger current flows out of the higher voltage cells, and a smaller current flows out of the lower voltage cells,

by which the any-cells-to-any-cells equalization for Module II is automatically achieved based on forward conversion.

The primary voltage of Transformer II  $V_{TP2j}$  can be given as

$$V_{TP2j} = V_{B2j} + L_{eqP2j} \cdot \frac{di_{B2j}}{dt} + R_{eqP2j} \cdot i_{B2j}, \quad (16)$$

where  $j = 1, 2, \dots, 4$ .  $V_{B2j}$  is the cell voltage of  $B_{2j}$  in Module II.  $i_{B2j}$  is the balancing current of  $B_{2j}$ .  $L_{eqP2j}$  represents the leakage inductance on a primary winding of Transformer II.  $R_{eqP2j}$  represents the equivalent resistance on a primary winding of Transformer II.

From (16), the primary balancing current  $i_{B2j}(t)$  can be derived as

$$i_{B2j}(t) \approx \frac{V_{M2} - 4V_{B2j}}{4L_{eqP2j}} \cdot (t - t_2). \quad (17)$$

Based on (17), Fig. 6 shows the primary balancing current  $i_{B24}$ , which declines linearly from zero.

During this mode, the loop equation in the secondary sides of the transformers can be represented by

$$V_{TS1} + V_{TS2} + (L_{eqS1} + L_{eqS2}) \cdot \frac{di_{TS1}}{dt} + (R_{eqS1} + R_{eqS2}) \cdot i_{TS1} = 0. \quad (18)$$

From (5), (6), and (18), the primary voltage of Transformer I can be obtained by

$$V_{TP1} = -V_{TP2} - \frac{N_P}{N_S} \cdot (L_{eqS1} + L_{eqS2}) \cdot \frac{di_{TS1}}{dt} - \frac{N_P}{N_S} \cdot (R_{eqS1} + R_{eqS2}) \cdot i_{TS1}. \quad (19)$$

In the secondary sides, when  $Q_{11} - Q_{14}$  are turned off,  $i_{L_{m1}}$  flow continuously, which forces the secondary current  $i_{TS1}$  rises instantaneously, as shown in Fig. 6. This resets Transformer I without using any additional demagnetizing circuits. By (18), the secondary balancing current  $i_{TS1}(t)$  can be approximately calculated as

$$i_{TS1}(t) \approx i_{TS1}(t_2) - \frac{n}{4} \cdot \frac{V_{M2} - V_{M1}}{L_{eqS1} + L_{eqS2}} \cdot (t - t_2). \quad (20)$$

Since  $V_{M2} - V_{M1} > 0$ ,  $i_{TS1}(t)$  will decrease linearly with a constant slope.

The magnetizing currents  $i_{L_{m1}}(t)$  and  $i_{L_{m2}}(t)$  in Transformer I and Transformer II can be given by

$$i_{L_{m1}}(t) \approx i_{L_{m1}}(t_2) + \frac{n}{4} \cdot \frac{V_{M1}}{L_{m1}} (t - t_2), \quad (21)$$

$$i_{L_{m2}}(t) \approx \frac{n}{4} \cdot \frac{V_{M2}}{L_{m2}} (t - t_2). \quad (22)$$

As shown in Fig. 5(c), the secondary balancing current  $i_{TS1}$  comes completely from the magnetizing current  $i_{L_{m1}}$  in Transformer I, having

$$i_{TS1} = -i_{L_{m1}}. \quad (23)$$

The relationship among the magnetizing currents and the balancing currents in Module II can be expressed as follows

$$\frac{N_S}{N_P} \cdot (i_{L_{m1}} + i_{L_{m2}}) = - \sum_{j=1}^4 i_{B2j}. \quad (24)$$

The duration of this mode is very short, and the main function of this mode is to achieve the demagnetization of Transformer I when switches  $Q_{11} - Q_{14}$  are turned off.

**Mode IV** ( $t_3 - t_4$ ): This mode does not start until the secondary current  $i_{TS1}$  changes its direction at  $t_3$ , as shown in Fig. 5(d). During this mode, the cell equalization in the primary sides of Module II still goes on. In the secondary sides, the magnetizing currents  $i_{L_{m1}}$  and  $i_{L_{m2}}$  are built up, by which the energy of Module II is stored into the magnetizing inductances  $L_{m1}$  and  $L_{m2}$ . This provides the pre-conditions for the equalization between the two modules without the need of additional balancing circuits.

In the secondary sides of the transformers, a loop equation can be achieved by

$$V_{TS1} + V_{TS2} + (L_{eqS1} + L_{eqS2}) \cdot \frac{di_{TS1}}{dt} - (R_{eqS1} + R_{eqS2}) \cdot i_{TS1} = 0. \quad (25)$$

From (5), (6), and (25), the primary voltage of Transformer I can be calculated as

$$V_{TP1} = -V_{TP2} - \frac{N_P}{N_S} \cdot (L_{eqS1} + L_{eqS2}) \cdot \frac{di_{TS1}}{dt} + \frac{N_P}{N_S} \cdot (R_{eqS1} + R_{eqS2}) \cdot i_{TS1}. \quad (26)$$

By solving (25), we can get the secondary balancing current  $i_{TS1}(t)$

$$i_{TS1}(t) \approx -\frac{n}{4} \cdot \frac{V_{M2} - V_{M1}}{L_{eqS1} + L_{eqS2}} \cdot (t - t_3). \quad (27)$$

The magnetizing currents  $i_{L_{m1}}$  and  $i_{L_{m2}}$  can be expressed as

$$i_{L_{m1}}(t) \approx \frac{n}{4} \cdot \frac{V_{M1}}{L_{m1}} \cdot (t - t_3), \quad (28)$$

$$i_{L_{m2}}(t) \approx i_{L_{m2}}(t_3) + \frac{n}{4} \cdot \frac{V_{M2}}{L_{m2}} \cdot (t - t_3). \quad (29)$$

The secondary balancing current is given by

$$i_{TS1} = -i_{L_{m1}}. \quad (30)$$

The main function of this mode is to achieve the equalization among the cells in Module II and the energy storage from Module II into magnetizing inductances  $L_{m1}$  and  $L_{m2}$ .

According to the above operating modes, magnetizing currents  $i_{L_{m1}}$  and  $i_{L_{m2}}$  can flow naturally between the two multi-winding transformers, which confirms the advantages of the proposed MAE without the need of additional demagnetizing circuits for the transformers.

### C. Consideration for Transformers

The switch frequency  $f$ , duty cycle  $D$ , turns ratio  $n$ , and magnetizing inductance  $L_m$  are the key design parameters of the

multi-winding transformers. It is assumed that the maximum cell voltage  $V_{max}$  is 4.2 V, the minimum cell voltage  $V_{min}$  is 3 V, the peak equalizing current  $i_{peak} \leq 1$  A, and the switching frequency is set as 25 kHz.

1) *Duty Cycle D*: The balancing between the two modules is based on flyback conversion. The relationship between the secondary voltages of the two transformers is determined by

$$\frac{V_{TS1}(I, II)}{V_{TS2}(III, IV)} = \frac{N_{S1}}{N_{P1}} \cdot \frac{N_{P2}}{N_{S2}} \cdot \frac{1-D}{D}, \quad (31)$$

where  $V_{TS1}(I, II)$  represents the secondary voltage of Transformer I during Modes I and II.  $V_{TS2}(III, IV)$  represents the secondary voltage of Transformer II during Modes III and IV.  $N_{S1}$  is the turn number of the secondary winding of Transformer I.  $N_{P1}$  is the turn number of the primary windings of Transformer I.  $N_{S2}$  is the turn number of the secondary winding of Transformer II.  $N_{P2}$  is the turn number of the primary windings of Transformer II.

Equation (31) can be deduced as

$$D = \frac{n_1 \cdot V_{TS2}(III, IV)}{n_2 \cdot V_{TS1}(I, II) + n_1 \cdot V_{TS2}(III, IV)}, \quad (32)$$

where  $n_1$  and  $n_2$  are the turns ratios of Transformers I and II, respectively, and can be expressed as

$$n_1 = \frac{N_{S1}}{N_{P1}}, \quad (33)$$

$$n_2 = \frac{N_{S2}}{N_{P2}}. \quad (34)$$

In order to achieve the voltage equalization between modules, the secondary voltages of Transformers I and II should satisfy

$$V_{TS1}(I, II) = V_{TS2}(III, IV). \quad (35)$$

By (32) and (35), the duty cycle  $D$  can be obtained as

$$D = \frac{n_1}{n_1 + n_2}. \quad (36)$$

Equation (36) shows the duty cycle only depends on the turns ratios of the transformers to achieve the balancing between modules. When the transformers have the same parameters, i.e.,  $n = n_1 = n_2$ ,  $D$  is calculated as 50%.

In addition, to prevent a reverse current flowing from the low voltage module to the high voltage one, the flyback converters should be operated in continuous current mode [24]. Thus, the duty cycle  $D$  should also satisfy

$$\begin{cases} DT \cdot n \cdot \frac{V_{max}}{L_{m1} + L_{eqS1}} - (1-D)T \cdot n \cdot \frac{V_{min}}{L_{m2} + L_{eqS2}} \geq 0 \\ (1-D)T \cdot n \cdot \frac{V_{max}}{L_{m2} + L_{eqS2}} - DT \cdot n \cdot \frac{V_{min}}{L_{m1} + L_{eqS1}} \geq 0 \end{cases}, \quad (37)$$

where  $T$  is the switching period.  $n$  is the turns ratio of the transformers.

By solving (37),  $D$  can be derived as

$$41.7\% \leq D \leq 58.3\%. \quad (38)$$

Therefore, the duty cycle  $D$  should be set as 50% to simultaneously achieve the balancing between modules and the continuous current mode of the flyback converters.

TABLE I  
PARAMETERS OF THE MULTI-WINDING TRANSFORMERS

	Transformer I					Transformer II				
	$TP_{11}$	$TP_{12}$	$TP_{13}$	$TP_{14}$	$TS_1$	$TP_{21}$	$TP_{22}$	$TP_{23}$	$TP_{24}$	$TS_2$
$L_m$ ( $\mu\text{H}$ )	158.1	157.6	157.7	157.5	2460	157.2	157.3	157.1	157.2	2480
$L_{eq}$ ( $\mu\text{H}$ )	0.24	0.23	0.22	0.21	36.7	0.29	0.28	0.34	0.34	39.6
$R_{eq}$ ( $\Omega$ )	0.52	0.51	0.52	0.51	7.53	0.51	0.51	0.51	0.52	7.82
$N_P$			17.5					17.5		
$N_S$			69.5					69.5		

2) *Turns Ratio  $n$* : According to Faraday's law, the primary windings of a transformer should have the same turn number to achieve the equalization among cells in a module. Moreover, according to (36), the transformers should also have the same turns ratio  $n$  and duty cycle  $D$  to achieve the equalization between modules. In fact, a large turns ratio  $n$  will result in a high secondary voltage and a small secondary current, leading to a low loss of the secondary winding but a bulk size and high cost. On the contrary, a small turns ratio  $n$  will result in a low secondary voltage and a large secondary current, leading to a high loss of the secondary winding but a small size and low cost. In general, the turns ratio  $n$  between 2–6 is a trade off among the circuit size, cost, and balancing efficiency for the proposed equalizer.

3) *Magnetizing Inductance  $L_m$* : To make full use of the transformers and prevent the core saturation, the peak charging/discharging current during any mode is limited to 1 A. The magnetizing inductance of the primary windings of the transformers can be obtained as follows [27]

$$L_m \geq \frac{V_{\max}}{|i_{\text{peak}}|} \cdot DT = 84 \mu\text{H}. \quad (39)$$

Actually, a large magnetizing inductance will weaken the effect of the flyback conversion and enhance the effect of the forward conversion. Conversely, a small magnetizing inductance will enhance the effect of the flyback conversion and weaken the effect of the forward conversion. Therefore, too large or too small magnetizing inductance will result in a reduction in the balancing performance. Thus, the magnetizing inductance of the primary windings is optimal to be between 100–200  $\mu\text{H}$ , and the magnetizing inductance of the secondary windings is preferred to be between 1600–3200  $\mu\text{H}$ .

From the above analyses, it can be concluded that as long as the multi-winding transformers have the same turns ratio and the same duty cycle, i.e.,  $D = 50\%$ , the proposed equalizer can achieve an ideal balancing effect for a battery string. According to (1) and (16), the battery internal resistance, MOSFET on-resistance, parasitic capacitance, and leakage inductance only affect the balancing current, not the final balanced voltage of the battery string.

### III. EXPERIMENTAL RESULTS

To certify the feasibility of the proposed MAE, a prototype for eight lithium-ion cells, which are divided into two modules, was implemented. Fig. 7 shows a picture of the experimental

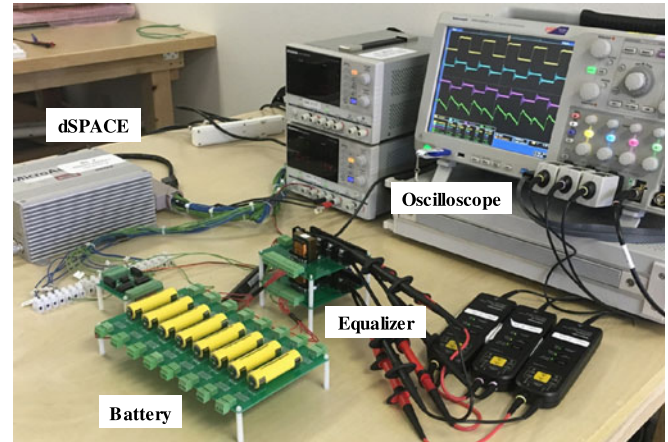


Fig. 7. Photograph of the implemented prototype and associated instruments.

prototype and the associated instruments. STP220N6F7 MOSFETs with 2.4-m $\Omega$  on-resistance were used for the switches  $Q_{11} - Q_{14}$  and  $Q_{21} - Q_{24}$ . dSPACE was used for the digital controller. Eight 1100-mAh LiFePO<sub>4</sub> batteries and eight 2600-mAh LiNiMnCoO<sub>2</sub> batteries were used during experiments. The parameters of the multi-winding transformers are summarized in Table I.

Fig. 8 shows the experimental waveforms for Module I and Module II at the frequency of  $f = 25$  kHz. All of the switches in Module I are driven by PWM+, and all of the switches in Module II are driven by the complementary signal PWM-. The battery cell voltages meet  $V_{B24} > V_{B23} > V_{B22} > V_{B21} > V_{B14} > V_{B13} > V_{B12} > V_{B11}$ .

Fig. 8(a) shows the primary voltage, current, and voltage stress on MOSFET switch  $Q_{11}$ . When  $Q_{11}$  are turned on, balancing current  $i_{B11}$  flows from the multi-winding transformer to the battery cell  $B_{11}$ . Due to the voltage difference between the primary voltage and the cell voltage applied to the leakage inductance  $L_{eq11}$ ,  $i_{B11}$  increases linearly from 0 to 70 mA. When  $Q_{11}$  is turned off, the maximum voltage stress on  $Q_{11}$  does not exceed 20 V even in the voltage spikes, reducing dv/dt of the MOSFETs regardless of the cell number.

Fig. 8(b) shows the primary voltages and currents of Module I and II. It can be observed that the equalization in Module I and Module II is executed in different half periods. Battery cell  $B_{11}$  is charged during a half period with the peak current of about 80 mA, and battery cell  $B_{24}$  is discharged during the other half period with the peak current of about 60 mA. According to (3)

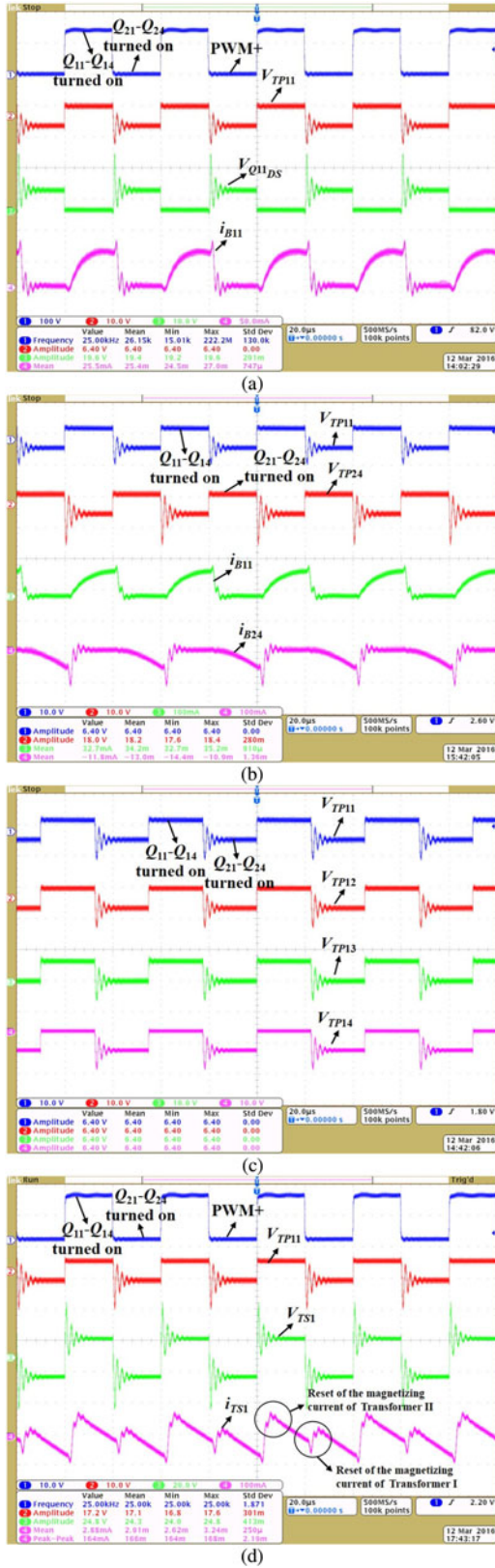


Fig. 8. Experimental waveforms for Module I and Module II. (a) The primary voltage and current in Module I. (b) The primary voltages and currents in Module I and Module II. (c) The four primary voltages in Module I. (d) The secondary voltages and secondary current.

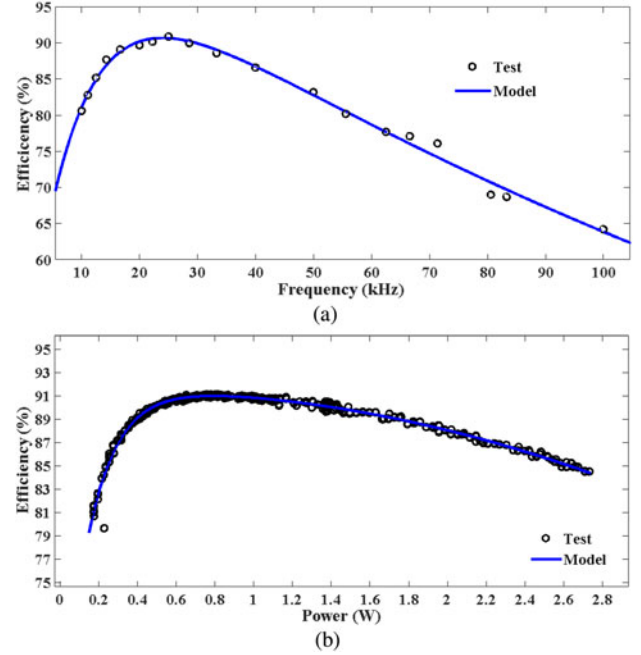


Fig. 9. Measured balancing efficiency  $\eta_e$ . (a) Measured efficiency  $\eta_e$  as a function of frequency. (b) Measured efficiency  $\eta_e$  as a function of power at the frequency of  $f = 25$  kHz.

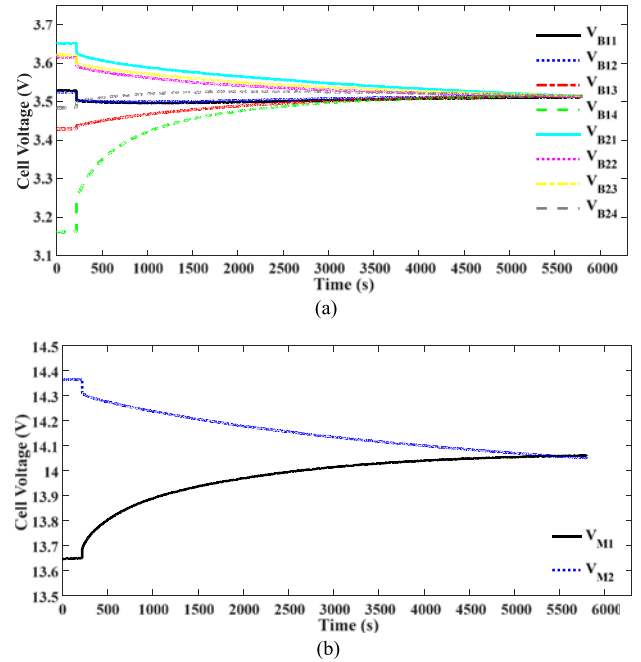


Fig. 10. Experimental results for eight LiNiMnCoO<sub>2</sub> cells at  $f = 25$  kHz, which are divided into two four-cell modules. (a) The cell voltage trajectories. (b) The module voltage trajectories.

and (17), the calculated peak currents are about 89 and 67 mA, respectively, which verifies the theoretical analyses.

Fig. 8(c) presents the four primary voltages in Module I. It can be observed that the four primary voltages are completely equal, i.e., about 3.2V, which proves the correctness of (2).

Fig. 8(d) shows the secondary voltages and current. During  $Q_{11} - Q_{14}$  turned-on period, the secondary voltage of the first

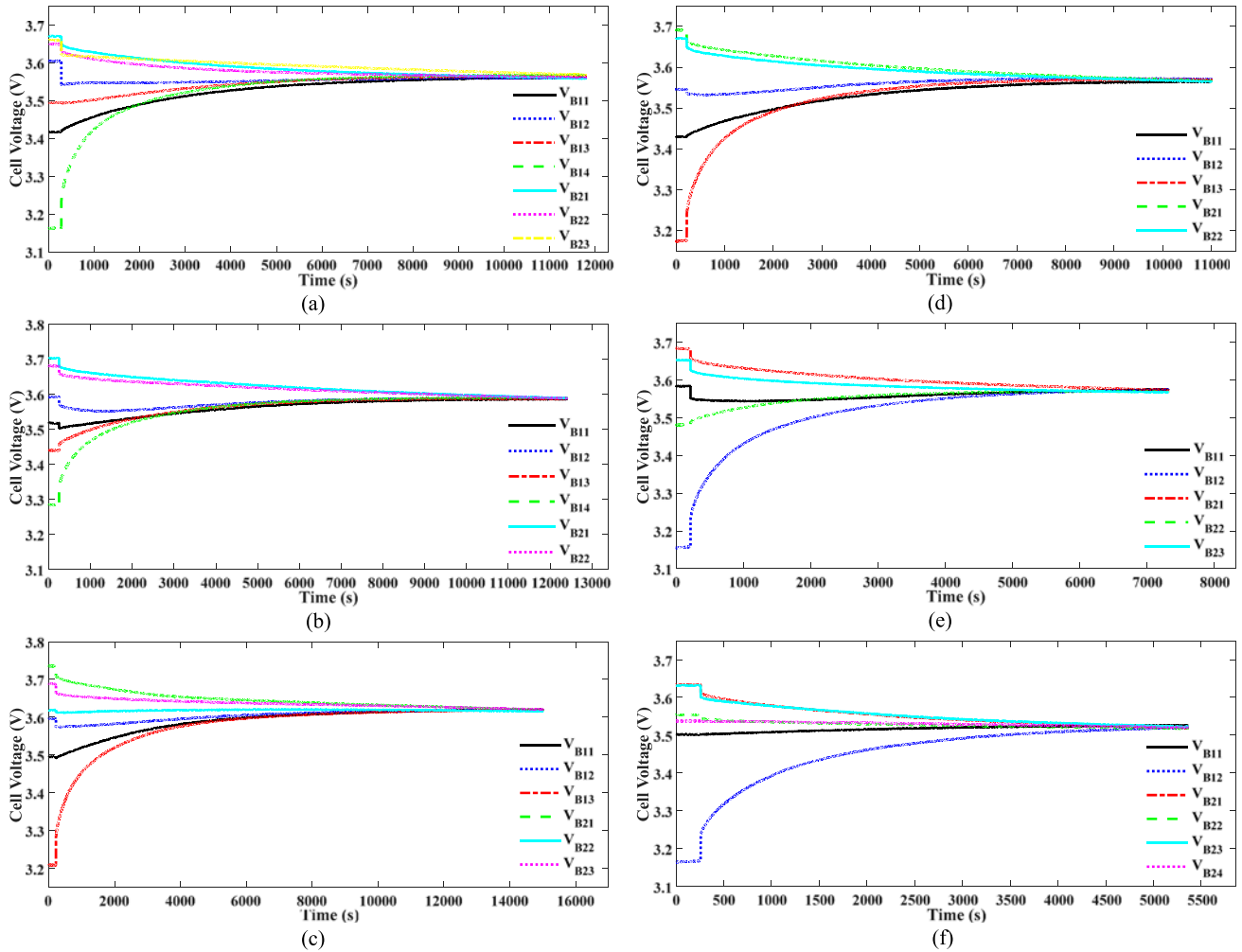


Fig. 11. Experimental results with unequal cell numbers in different modules at  $f = 25$  kHz. (a) 4 cells in Module I and 3 cells in Module II. (b) 4 cells in Module I and 2 cells in Module II. (c) 3 cells in Module I and 3 cells in Module II. (d) 3 cells in Module I and 2 cells in Module II. (e) 2 cells in Module I and 3 cells in Module II. (f) 2 cells in Module I and 4 cells in Module II.

TABLE II  
BALANCING RESULTS WITH UNEQUAL CELL NUMBERS IN THE TWO MODULES

Fig. 11	(a)	(b)	(c)	(d)	(e)	(f)
Balancing time (s)	12 000	12 420	15 000	11 000	7326	5360
Balanced voltage (V)	3.566	3.587	3.618	3.567	3.572	3.521
Voltage gap after balancing (mV)	9	4	6	7	7	9

transformer is built up and the secondary current flows from the second transformer to the positive polarity of the first transformer. This means that the energy stored in the second transformer is transferred to Module I, which achieves the voltage equalization between modules. During  $Q_{21} - Q_{24}$  turned-on period, the secondary voltage of the secondary transformer is built up and the secondary balancing current flows from the second transformer to the negative polarity of the first transformer. This means that the energy of Module II is delivered and stored into the magnetizing inductance of the first transformer. The measured peak-to-peak value of the secondary current is about 164 mA compared with the calculated value, i.e., 183 mA based

on (10) and (27). This result agrees well with the theoretical waveforms of the secondary voltages and current, which also proves that the demagnetization for the transformers can be automatically achieved without additional demagnetizing circuits.

Fig. 9(a) shows the balancing efficiency  $\eta_e$  as a function of frequency. Balancing efficiency  $\eta_e$  reaches the maximum value of 91% at the frequency of  $f = 25$  kHz, and then decreases as the frequency increases from 25 to 100 kHz. Fig. 9(b) shows the balancing efficiency  $\eta_e$  as a function of power at the frequency of  $f = 25$  kHz. It can be seen that efficiency  $\eta_e$  increases from 80.7% to 91.3% as the increase of the output power from 0.176 to 0.812 W. However,  $\eta_e$  decreases from 91.3% to 84.5% when the output power continues to increase to 2.733 W. Therefore, the proposed MAE achieves a high balancing efficiency over a wide range of frequencies and loading conditions.

Fig. 10 shows the experimental results for eight LiNiMnCoO<sub>2</sub> cells at  $f = 25$  kHz. As shown in Fig. 10(a), the initial cell voltages are 3.528, 3.524, 3.429, 3.165, 3.652, 3.616, 3.621, and 3.483 V, respectively, and the maximum voltage gap is 0.487 V. It can be observed that all cell voltages converge simultaneously toward the average value, showing the any-cells-to-any-cells

TABLE III  
COMPARISON OF SEVERAL BATTERY EQUALIZERS

Battery equalizers	Components						Speed	Efficiency	Control simplicity	Modularization simplicity
	SW	R	L	C	D	T				
Dissipative equalizer [7]	$n$	$n$	0	0	0	0	L	L	M	M
Classical SC [8]	$2n$	0	0	$n-1$	0	0	L	M	H	L
Double-tiered SC [9]	$2n$	0	0	$n$	0	0	L	L	H	L
Switched-coupling-capacitor [13]	$2n$	0	0	$n$	0	0	M	H	H	H
Adjacent cell-to-cell resonant SC [14]	$2n$	0	$n-1$	$n-1$	0	0	L	M	H	L
Direct cell-to-cell resonant SC [17]	$2(n+5x)$	0	$x$	$x$	0	0	M	M	L	L
Multiphase interleaved equalizer [19]	$2(n-1)$	0	$n-1$	0	0	0	M	M	H	L
Optimized next-to-next balancing [20]	$4(n-1)$	0	$2(n-1)$	0	0	0	M	M	H	L
Flyback converter [22]	$2(n-x)$	0	0	0	$2(n-x)$	$x$	M	M	L	L
Forward converter [28]	$n$	0	0	$n$	0	$x$	H	H	H	M
Forward or flyback converter [30]	$2n$	0	0	0	0	$x$	M	M	L	M
Forward-flyback converter [31]	$n$	0	0	0	0	$x$	H	M	H	H
Proposed modularized equalizer	$n$	0	0	0	0	$x$	H	H	H	H

$n$  is the number of cells in the battery string,  $x$  is the number of battery modules in the battery string. SC: Switched capacitor. SW: Switches. R: Resistors. L: Inductors. C: Capacitors. D: Diodes. T: Transformers.

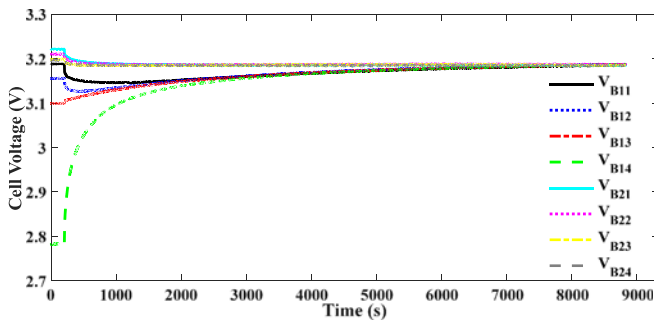


Fig. 12. Experimental result for eight LiFePO<sub>4</sub> cells at  $f = 25$  kHz.

balancing performance. After about 5800 s, a balanced voltage of 3.515 V is achieved with the voltage gap of 3 mV among cells. Fig. 10(b) shows the module voltage trajectories, which are equal at the end of the balancing.

Fig. 11 shows the experimental results with unequal cell numbers in different modules at  $f = 25$  kHz. We can observe that the voltage equalization for the cells and modules is effectively executed by the proposed MAE even though there are unequal numbers of cells in the two modules. Table II summarizes the balancing results. These results confirm that the good performance of the proposed MAE is not affected by the number of cells in modules and the combining forms of the forward and flyback conversions, demonstrating the simple modularization of the proposed equalizer.

In order to further verify the robustness of the proposed MAE, Fig. 12 shows the balancing result for eight LiFePO<sub>4</sub> cells at  $f = 25$  kHz. The initial cell voltages are set as 3.188, 3.156, 3.099, 2.782, 3.221, 3.21, 3.199, and 3.195 V, respectively. The initial maximum voltage gap among cells is about 0.439 V. After about 8898 s, a balanced voltage of 3.186 V is achieved with the voltage gap of 4 mV among cells. This result is consistent with that shown in Fig. 10, which proves the proposed MAE can also be applied to other rechargeable batteries without significant change or recalibration.

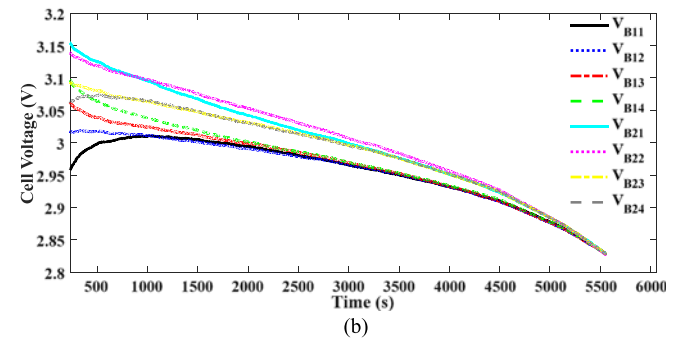
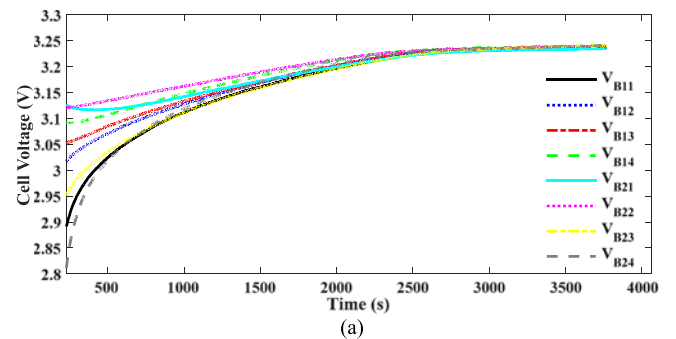


Fig. 13. Dynamic balancing results for eight LiFePO<sub>4</sub> cells. (a) Battery charge. (b) Battery discharge.

In order to prove the validity of the dynamic equalization of the proposed scheme, Fig. 13 shows the balancing results for an eight-LiFePO<sub>4</sub>-cell battery string during the constant-current charging and discharging. As shown in Fig. 13(a), the proposed equalizer converges the cell voltages together to ensure all cells identically charged. The maximum voltage gap among cells is reduced greatly from 315 to 7 mV. As shown in Fig. 13(b), due to the proposed scheme, all cells are simultaneously discharged to the cut-off voltage with the voltage gap reduced from 196 to 5 mV. It can be concluded that the proposed equalizer improves greatly the consistency and the available capacity of the battery

string during the charging and discharging, indicating a good dynamic balancing performance.

#### IV. COMPARISON WITH EXISTING EQUALIZERS

Table III illustrates a systematic comparison with existing battery equalizers in terms of the components, balancing speed, efficiency, control simplicity, and modularization simplicity. The evaluation criterions for the balancing speed and efficiency are presented in [31]. Besides, control simplicity is evaluated according to the control signal number, the complexity of generating the control signals, and the necessity of cell monitoring. Modularization simplicity is evaluated according to the number of elements for the balancing among modules and the expandability. The balancing performance parameters are divided into three scales, of which “H”, “M”, and “L” represents the high, medium, and low scales, respectively.

From Table III, it can be observed that the proposed equalizer has the obvious advantages of small size, low cost, high efficiency, fast balancing speed, and easy modularization because it shares one circuit for the balancing among cells and modules. In conclusion, the proposed topology can meet the most demands of a long series-connected battery string to be used in EVs.

#### V. CONCLUSION

The purpose of this paper is to introduce a modularization method for battery equalizers using multi-winding transformers. The configuration of the proposed modularized equalizer, the operation principles, the cell balancing performance, and the comparison with existing equalizers are presented. The proposed method does not need additional components for the equalization among modules and the demagnetization of the multi-winding transformers, resulting in a small size and low cost. Moreover, by driving all MOSFETs using two complementary PWM signals, the proposed equalizer can automatically and simultaneously deliver energy from any high voltage cells to any low voltage cells without the need of cell voltage sensors. In addition, a low voltage stress on all power devices is obtained, thereby ensuring the high reliability of the proposed balancing circuit. The practical implementation presented in this paper has shown the good balancing performances of the proposed equalizer with a simple control and a high balancing efficiency of 91.3%. Particularly, the modularization of the proposed equalizer is very simple and is not restricted by the number of cells in each module. Therefore, the proposed method is a good candidate for lithium-ion battery strings with hundreds of cells connected in series to be used in EVs.

#### REFERENCES

- [1] A. Lievre *et al.*, “Practical online estimation of lithium-ion batteries apparent series resistance for mild hybrid vehicles,” *IEEE Trans. Veh. Technol.*, vol. 65, no. 6, pp. 4505–4511, Jun. 2016.
- [2] J. Jaguemont, L. Boulon, P. Venet, Y. Dubé, and A. Sari, “Lithium-Ion battery aging experiments at subzero temperatures and model development for capacity fade estimation,” *IEEE Trans. Veh. Technol.*, vol. 65, no. 6, pp. 4328–4343, Jun. 2016.
- [3] B. Xia and C. Mi, “A fault-tolerant voltage measurement method for series connected battery packs,” *J. Power Sources*, vol. 308, pp. 83–96, Mar. 2016.
- [4] L. Lua, X. Hana, J. Lia, J. Huab, and M. Ouyanga, “A review on the key issues for lithium-ion battery management in electric vehicles,” *J. Power Sources*, vol. 226, pp. 272–288, 2013.
- [5] B. Xia, Y. Shang, T. Nguyen, and C. Mi, “A correlation based fault detection method for short circuits in battery packs,” *J. Power Sources*, vol. 337, pp. 1–10, Jan. 2017.
- [6] J. G.-Lozano and E. R. Cadaval, “Battery equalization active methods,” *J. Power Sources*, vol. 246, pp. 934–949, 2014.
- [7] G.-L. Javier, R.-C. Enrique, M.-M., M. Isabel, and G.-M. Miguel, “A novel active battery equalization control with on-line unhealthy cell detection and cell change decision,” *J. Power Sources*, vol. 299, pp. 356–370, 2015.
- [8] C. Pascual and P. T. Krein, “Switched capacitor system for automatic series battery equalization,” in *Proc. IEEE Appl. Power Electron. Conf.*, 1997, pp. 848–854.
- [9] A. C. Baughman and M. Ferdowsi, “Double-tiered switched-capacitor battery charge equalization technique,” *IEEE Trans. Ind. Electron.*, vol. 55, no. 6, pp. 2277–2285, Jun. 2008.
- [10] M.-Y. Kim, C.-H. Kim, J.-H. Kim, and G.-W. Moon, “A chain structure of switched capacitor for improve cell balancing speed of lithium-ion batteries,” *IEEE Trans. Ind. Electron.*, vol. 61, no. 8, pp. 3989–3999, Aug. 2014.
- [11] Y. Ye and K. W. E. Cheng, “Modeling and analysis of series-parallel switched-capacitor voltage equalizer for battery/supercapacitor strings,” *IEEE J. Emerg. Sel. Topics Power Electron.*, vol. 3, no. 4, pp. 977–983, Dec. 2015.
- [12] Y. Ye and K. W. E. Cheng, “An automatic switched-capacitor cell balancing circuit for series-connected battery strings,” *Energies*, vol. 9, no. 3, pp. 1–15, Feb. 2016.
- [13] Y. Shang *et al.*, “A switched-coupling-capacitor equalizer for series-connected battery strings,” *IEEE Trans. Power Electron.*, vol. 32, no. 10, pp. 7694–7706, Oct. 2017.
- [14] Y. Ye, K. W. E. Cheng, and Y. P. B. Yeung, “Zero-current switching switched-capacitor zero-voltage-gap automatic equalization system for series battery string,” *IEEE Trans. Power Electron.*, vol. 27, no. 7, pp. 3234–3242, Jul. 2012.
- [15] Y. Shang, C. Zhang, N. Cui, and J. M. Guerrero, “A cell-to-cell battery equalizer with zero-current switching and zero-voltage gap based on quasi-resonant LC converter and boost converter,” *IEEE Trans. Power Electron.*, vol. 30, no. 7, pp. 3731–3747, Jul. 2015.
- [16] Y. Shang, C. Zhang, N. Cui, and J. M. Guerrero, “A crossed pack-to-cell equalizer based on quasi-resonant LC converter with adaptive fuzzy logic equalization control for series-connected lithium-ion battery strings,” in *Proc. IEEE Appl. Power Electron. Conf.*, 2015, pp. 1685–1692.
- [17] K. Lee, Y. Chung, C.-H. Sung, and B. Kang, “Active cell balancing of li-ion batteries using LC series resonant circuit,” *IEEE Trans. Ind. Electron.*, vol. 62, no. 9, pp. 5491–5501, Sep. 2015.
- [18] Y. Shang, Q. Zhang, N. Cui, and C. Zhang, “A cell-to-cell equalizer based on three-resonant-state switched-capacitor converters for series-connected battery strings,” *Energies*, vol. 10, no. 2, pp. 1–15, Feb. 2017.
- [19] F. Mestrallet, L. Kerachev, J.-C. Crebier, and A. Collet, “Multiphase interleaved converter for lithium battery active balancing,” *IEEE Trans. Power Electron.*, vol. 29, no. 6, pp. 2874–2881, Jun. 2014.
- [20] T. H. Phung, A. Collet, and J.-C. Crebier, “An optimized topology for next-to-next balancing of series-connected lithium-ion cells,” *IEEE Trans. Power Electron.*, vol. 29, no. 9, pp. 4603–4613, Sep. 2014.
- [21] M.-Y. Kim, J.-H. Kim, and G.-W. Moon, “Center-cell concentration structure of a cell-to-cell balancing circuit with a reduced number of switches,” *IEEE Trans. Power Electron.*, vol. 29, no. 10, pp. 5285–5297, Oct. 2014.
- [22] A. M. Imitiaz and F. H. Khan, “Time shared flyback converter” based regenerative cell balancing technique for series connected li-ion battery strings,” *IEEE Trans. Power Electron.*, vol. 28, no. 12, pp. 5960–5975, Dec. 2013.
- [23] C. Hua and Y.-H. Fang, “A charge equalizer with a combination of APWM and PFM control based on a modified half-bridge converter,” *IEEE Trans. Power Electron.*, vol. 31, no. 4, pp. 2970–2979, Apr. 2016.
- [24] C.-S. Lim, K.-J. Lee, N.-J. Ku, D.-S. Hyun, and R.-Y. Kim, “A modularized equalization method based on magnetizing energy for a series-connected lithium-ion battery string,” *IEEE Trans. Power Electron.*, vol. 29, no. 4, pp. 1791–1799, Apr. 2014.

- [25] C.-H. Kim, M.-Y. Kim, and G.-W. Moon, "A modularized charge equalizer using a battery monitoring IC for series-connected Li-ion battery strings in electric vehicles," *IEEE Trans. Power Electron.*, vol. 28, no. 8, pp. 3779–3787, Aug. 2013.
- [26] M. Uno and A. Kukita, "Double-switch equalizer using parallel-or series-parallel-resonant inverter and voltage multiplier for series-connected supercapacitors," *IEEE Trans. Power Electron.*, vol. 29, no. 2, pp. 812–828, Feb. 2014.
- [27] M. Arias, J. Sebastián, M. Hernando, U. Viscarret, and I. Gil, "Practical application of the wave-trap concept in battery-cell equalizers," *IEEE Trans. Power Electron.*, vol. 30, no. 10, pp. 5616–5631, Oct. 2015.
- [28] S. Li, C. Mi, and M. Zhang, "A high-efficiency active battery-balancing circuit using multiwinding transformer," *IEEE Trans. Ind. Appl.*, vol. 49, no. 1, pp. 198–207, Jan. 2013.
- [29] M. Uno and K. Akio, "Single-switch single-transformer cell voltage equalizer based on forward-flyback resonant inverter and voltage multiplier for series-connected energy storage cells," *IEEE Trans. Veh. Technol.*, vol. 63, no. 9, pp. 4232–4247, Nov. 2014.
- [30] Y. Chen, X. Liu, Y. Cui, J. Zou, and S. Yang, "A multi-winding transformer cell-to-cell active equalization method for lithium-ion batteries with reduced number of driving circuits," *IEEE Trans. Power Electron.*, vol. 31, no. 7, pp. 4916–4929, Jul. 2016.
- [31] Y. Shang *et al.*, "An automatic equalizer based on forward-flyback converter for series-connected battery strings," *IEEE Trans. Ind. Electron.*, to be published, DOI 10.1109/TIE.2017.2674617, 2017.
- [32] H.-S. Park, C.-H. Kim, K.-B. Park, G.-W. Moon, and J.-H. Lee, "Design of a charge equalizer based on battery modularization," *IEEE Trans. Veh. Technol.*, vol. 58, no. 7, pp. 3216–3223, Sep. 2009.
- [33] B. Dong, Y. Li, and Y. Han, "Parallel architecture for battery charge equalization," *IEEE Trans. Power Electron.*, vol. 30, no. 9, pp. 4906–4913, Sep. 2015.



**Chenghui Zhang** (M'14) received the Bachelor's and Master's degrees in automation engineering and the Ph.D. degree in control theory and operational research from Shandong University of Technology, Jinan, China, in 1985, 1988, and 2001, respectively. In 1988, he joined Shandong University, where he is currently a Professor of School of Control Science and Engineering at Shandong University, the Chief Manager of Power Electronic Energy-saving Technology & Equipment Research Center of Education Ministry, a Specially Invited Cheung Kong Scholars Professor by China Ministry of Education, and a Taishan Scholar Special Adjunct Professor. He is also one of state-level candidates of "the New Century National Hundred, Thousand and Ten Thousand Talent Project," the Academic Leader of Innovation Team of Ministry of Education, and the Chief Expert of the National "863" high technological planning. His research interests include optimal control of engineering, power electronics and motor drives, energy-saving techniques, and time-delay systems.



**Naxin Cui** (M'14) received the B.S. degree in automation from Tianjin University, Tianjin, China, in 1989, and the M.S. and Ph.D. degrees in control theory and applications from Shandong University, Jinan, China, in 1994 and 2005, respectively.

In 1994, she joined Shandong University, where she is currently a Full Professor in the School of Control Science and Engineering. Her current research interests include power electronics, motor drives, automatic control theory and application, and battery energy management system of electric vehicles.



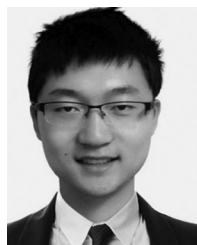
**Yunlong Shang** (S'14) received the B.S. degree in automation from Hefei University of Technology, Hefei, China, in 2008. Since 2010, he has been working toward the Ph.D. degree in the School of Control Science and Engineering, Shandong University, Shandong, China. In 2015, he received the funding from China Scholarship Council, and became a joint Ph.D. in the Department of Electrical and Computer Engineering, San Diego State University, California, USA.

His current research interests include the design and control of battery management systems and battery equalizers, battery modeling, and battery state estimation.



**Jufeng Yang** (S'15) received the B.S. degree in electrical engineering in 2012 from Nanjing University of Aeronautics and Astronautics, Nanjing, China, where he is currently working toward the Ph.D. degree (master-doctorate program) in electrical engineering. In 2015, he received the funding from China Scholarship Council, and became a joint Ph.D. in the Department of Electrical and Computer Engineering, San Diego State University, San Diego, CA, USA.

His research interests focus on battery management systems, including battery modeling, battery model parameter identification, and battery state estimation.



**Bing Xia** (S'13) received the B.S. degree in mechanical engineering from the University of Michigan, Ann Arbor, MI, USA, and the B.S. degree in electrical engineering from Shanghai Jiaotong University, Shanghai, China, in 2012. He was a Ph.D. student in Automotive System Engineering at University of Michigan Dearborn between winter 2013 and summer 2015. Starting from Fall 2015, he is a Ph.D. candidate in the joint Ph.D. program with San Diego State University and University of California, San Diego, CA, USA.

His research interests focus on batteries, including charging optimization, battery safety, and battery management.



**Chunting Chris Mi** (S'00–A'01–M'01–SM'03–F'12) received the B.S.E.E. and M.S.E.E. degrees in electrical engineering from Northwestern Polytechnical University, Xi'an, China, in 1985 and 1988, respectively. He received the Ph.D. degree in electrical engineering from the University of Toronto, Toronto, ON, Canada in 2001.

He is currently a Professor and the Chair of Electrical and Computer Engineering and the Director of the Department of Energy-funded Graduate Automotive Technology Education (GATE) Center for Electric Drive Transportation, San Diego State University, San Diego, CA, USA. Prior to joining SDSU, he was with in the University of Michigan, Dearborn, MI, USA, from 2001 to 2015.

His research interests include electric drives, power electronics, electric machines, renewable-energy systems, and electrical and hybrid vehicles. He has conducted extensive research and has published more than 100 journal papers.